ISSN 1814-4225 (print)
ISSN 2663-2012 (online)

UDC 629.735.33.028:621.884:620.179.1 **doi: 10.32620/reks.2021.3.08**

A. VERTIY[1], V. UCHANIN[2], V. PAVLIKOV[1], S. ZHYLA[1], O. SHMATKO[1], E. TSERNE[1]

[1] *National Aerospace University "Kharkiv Aviation Institute", Ukraine*
[2] *Karpenko Physico-Mechanical Institute of National Academy of Sciences of Ukraine, Lviv, Ukraine*

EDDY CURRENT TOMOGRAPHY FOR VISUALIZATION OF CRACKS IN AIRCRAFT RIVETED JOINTS

The control of the subsurface areas of metal products is necessary in many technological processes. So, for example, in aerospace technology it is essential to determine the presence of defects in aircraft engines. The same problems arise in chemical, power and other industries, which are letting out the highly technological equipment one of the widely known methods for inspecting metal products in the aviation industry is the eddy current method. This method is widely used to control small microscopic defects inside conductive materials. This method allows to ensure the safety of the operation of various products and devices in many areas of modern industry. An eddy current detector (probe) is a device, which induces eddy currents into metal objects and then detects the magnetic fields produced by these eddy currents. A magnetic field is created by a coil, or set of coils, through which a time-varying electrical current is driven. The frequency regime is sufficiently low, a few hertz to a few hundred kilohertz, so the targets of interest are within the near field of the transmitter. Considering the high conductivity of study samples, we can define that used waves in metals are located in the millimeter wave band. An eddy current imaging can be considered near-field imaging and a device allowing obtaining the eddy current images as a scanning near-field microscope. The obtained experimental results showed that the proposed tomographic method is effective for studying various complex inhomogeneities under the metal surface.

Keywords: *eddy current tomography; multi-frequency mode; subsurface imaging.*

Introduction

The control of the subsurface areas form of the metal products is necessary for many technological processes. So, for example, for aviation technologies, it is very important to determine the presence of defects in the metal components of flying devices. The same problems arise in chemical, power, and other industries, which are letting out the highly technological equipment. The various methods [1] are used for the detection of the subsurface defects (cracks, breaks, and other irregularities) in the metal products. Among them, the important place is occupied by electromagnetic methods, in which a very wide range of signals (from X-ray to signals with frequency ~ of tens hertz) is used [2-4]. Widely used electromagnetic methods of the control of defects in the metal products now is the methods allowing to restore unknown distribution conductivity in the researched area of metal from the measured electrical characteristics test (a frame, a coil), scanning space above a surface of a metal, in which the electrical currents (eddy currents) are exited [5, 7, 8]. Methods of calculation and analysis of the eddy currents behavior in the metal structures are considered in works [9-11]. Methods of inverse problems solution of in eddy current testing are presented in [12, 13].

An eddy current model for three-dimensional inversion was considered in [12]. The model is presented for the inversion of the eddy current date to be used for the detection of flaws. This model is based on rigorous electromagnetic theory and uses a multifrequency approach to make it truly three-dimensional. The resulting integral equations are discretized and solved using least-squares techniques [14-16]. The numerical problems involved in this algorithm are discussed and a solution, as well as examples of reconstructions of the computer-generated flaws, is presented.

Most widely eddy current flaw reconstruction strategies are based on the minimization of a nonlinear least-squares error functional. The theory of eddy current inversion has been considered in [13]. Then where developed for problems with an arbitrary specimen, probe, and defect shapes. A fast 3D forward solver is created to rapidly predict eddy current signals in the inversion shell. The high speed of the signal evaluation comes by utilizing a reaction data set constructed before performing the inversion by a finite element electromagnetic field simulator. The same pre-calculated reaction data set supports the quick evaluation of sensitivity information, thereby ensuring the efficient implementation of an optimization algorithm. Two general types of inverse problems are considered: the reconstruction of a

conductivity distribution and the reconstruction of the shape of inclusion or crack whose conductivity is known or assumed to be zero.

Paper [14] presents inverse analysis by using Boundary Element Method (BEM) with Laplace transform including the terminal voltage method. The method is applied to a simple problem in the eddy current testing (ECT). Some crack shapes in a conductive specimen are estimated from distributions of the transient eddy current on its sensing surface and magnetic flux density in the liftoff space. Because the transient behavior includes information on various frequency components, the method applies to the shape estimation of a comparative small crack.

The deconvolution algorithms applied to the measured data are described in papers [15]. In the work [15] was shown that the connectivity of surface-breaking structures whose overall size is comparable to that of the transducer could be extracted from eddy current data by the application of image processing techniques. Specially designed probes and image processing can be combined for scanning at increased rates to cover greater areas for high-resolution scanning for automatic extraction of quantitative detail or the enhanced probability of flaw detection. The interaction of the eddy current probe with the surface structure can be represented as a convolution of the point-spread function with the structure. Processing steps described in [15] involve: background removal to improve the signal to noise; smoothing or tapering of the image edges to reduce Gibbs' phenomena; insertion of both the point spread function and the blurred image into large zero images to eliminate aliasing, and then restoring the shape of the surface structure with a Wiener filter. The point-spread function is found by scanning the probe over a small symmetrical artifact, such as a deep hole of 0.25 mm diameter. The data was obtained at 500 kHz. The restored image is the inverse Fourier transform of the Wiener filter applied to the degraded image. Other important methods used in electromagnetic field inversion are described in [17].

Approach [18, 19] for imaging the anomaly (actually, the eddy currents induced within) can be made via almost straightforward application of a scalar, FFT – based diffraction tomography procedure, which was initially developed for microwave and ultrasonic imaging of buried targets. Eddy Current Imaging Method via diffraction tomography procedure starts from the equation, which yields the anomalous field on the probing line as a function of the eddy currents induced within the anomaly. So the eddy current problem will be solved if it will be found the inverse transform of this equation. Authors of works [18, 19] suggest doing it by different methods. Some of the modeling results are presented in these works. They show possibilities and limits of the eddy current tomography using modeling.

Scanning near-field microscopy was first demonstrated at microwave frequencies in [20] with a resolution of $\sim \lambda/60$. Near-field imaging has been accomplished in a variety of instruments, which cover frequencies spanning the microwave to optical regions. For example, authors of work [21] describe a novel type of scanning near-field millimeter-wave microscopy using a metal slit of the end of a tapered rectangular waveguide as a scanning probe and an image reconstruction algorithm based on the computer tomography imaging. Experiments performed at 60 GHz ($\lambda = 5mm$) show that two-dimensional near-field intensity images can be obtained with a resolution of $82\mu m$ ($\sim \lambda/60$). In the case of strongly attenuating environments like a damaged metallic structure where eddy currents are generated there is one key question how to deal with evanescent waves. A similar question arises when the super-resolution of a scatterer is aimed at by using the evanescent spectrum of its near field. Most current diffraction tomography reconstruction methods have been developed for the far-field, ignoring the near-field phenomenon of evanescent fields. These evanescent fields, which decay exponentially as the distance from the scattering object, carry high spatial frequency information. Thus, when operating in the near field, they can be included in a reconstruction algorithm to achieve higher resolution reconstructions.

The results of electromagnetic simulation on imaging of the subsurface objects are given in the paper [23]. Objects investigated are dielectric cylinders embedded into the dielectric homogeneous half-space lossy. It was supposed that objects have weak contrast. For image reconstruction of objects, a plane wave spectrum of back-scattered field is used.

The present work demonstrates the experimental eddy current near-field microscopy results obtained for the metal samples by using the tomography imaging method.

Detection of cracks on rivet junctions by using eddy current tomography

The Eddy current tomography [22, 24, 27] is a unique technology for 3-D subsurface imaging of voids and cracks in metals. The main aim of the study is to show the eddy current tomography possibilities and detect cracks on the demo panel. It is well known, that the modern eddy current industry has many special techniques for detecting different cracks in complex metallic elements such as, for example, rivet junctions and others. It is necessary to take into account that the presented below experimental results have been obtained using of standard "Nortec"- eddy current absolute

ISSN 1814-4225 (print)
ISSN 2663-2012 (online)

probe and 2-d linear scanner. But one feature is presented in this method. The eddy current device works at multi-frequency mode. About 16 frequencies in the wideband are used for tomography processing. Moreover, no previous special filtration is used that takes place in the case of fast-rotating or moving of eddy current probes relative to the investigated specimen.

Experimental eddy current tomography setup is presented in Fig. 1. The setup consists of a PC laptop, step motor control block, eddy current device (multi-frequency mode), and slow 2-d linear scanner. PC laptop controls all measuring equipment. A demo panel is used as a specimen. Digitized raw data of 16 frequencies come to PC laptop where eddy current tomography is processed. The principle of scanning is shown below in Fig. 2. Two-way scanning has been done. It minimizes measurement time and data acquiring. The scanning field has been studied for each riveted joint. The scanning area was 10 mm by following X-coordinate and 15 mm by following Y-coordinate. Ways of eddy current probe symbolically are shown as a black dash line. Photos of the eddy current tomography experimental setup with the demo panel under investigation are presented in Fig. 3. The left side picture shows a common view of the setup. The right photo gives the eddy current probe that is moving over the rivet junction. Experimental measurements have been done in several stages. Firstly, the possibility of the presented eddy current tomography experimental setup for testing of the rivet type junction has been investigated using only tomography technologies. The simplified schematic diagram of the open rivet junction is shown in Fig. 4. As it is shown below, a truss-head type of rivet is used for assembling the two parts of the demo panel. Such kind of rivet has some part that goes over the panel surface. The part may cause additional local unnecessary parasitic signal during the time while probe will pass near it. A special tip for the eddy current probe reduces a parasitic signal to a minimum. The next schematic diagram of the already covered rivet junction is shown in Fig. 5.

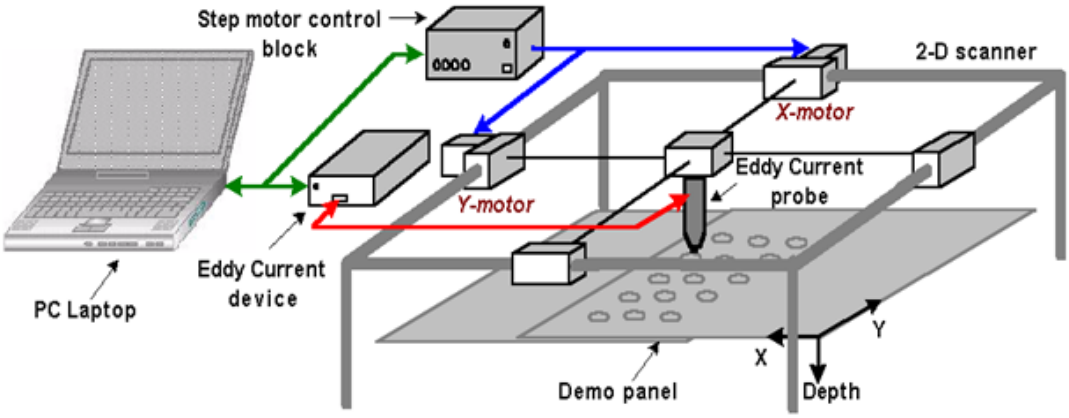

Fig. 1. Scheme of eddy current tomography experimental setup

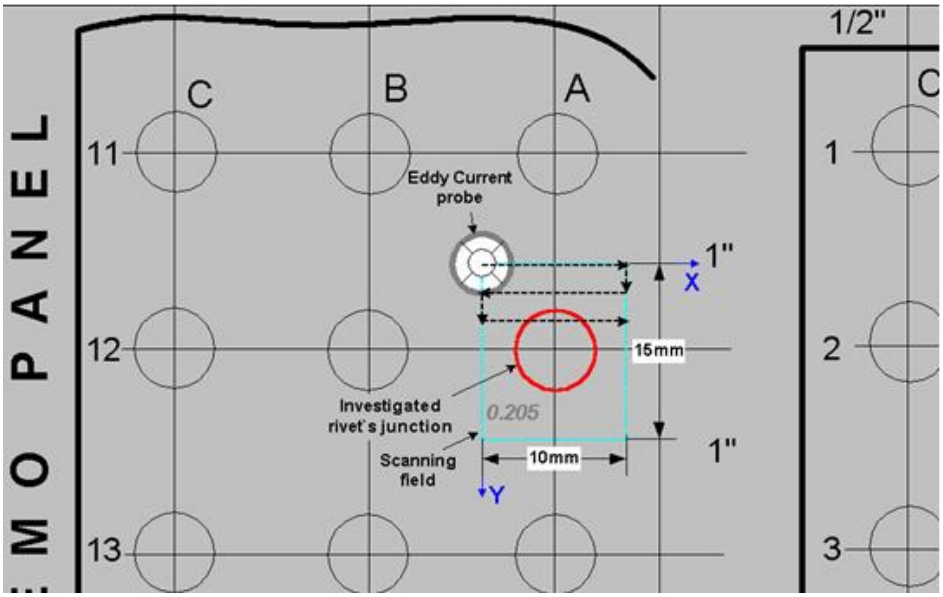

Fig. 2. Two-way Eddy Current scanning of rivet junction

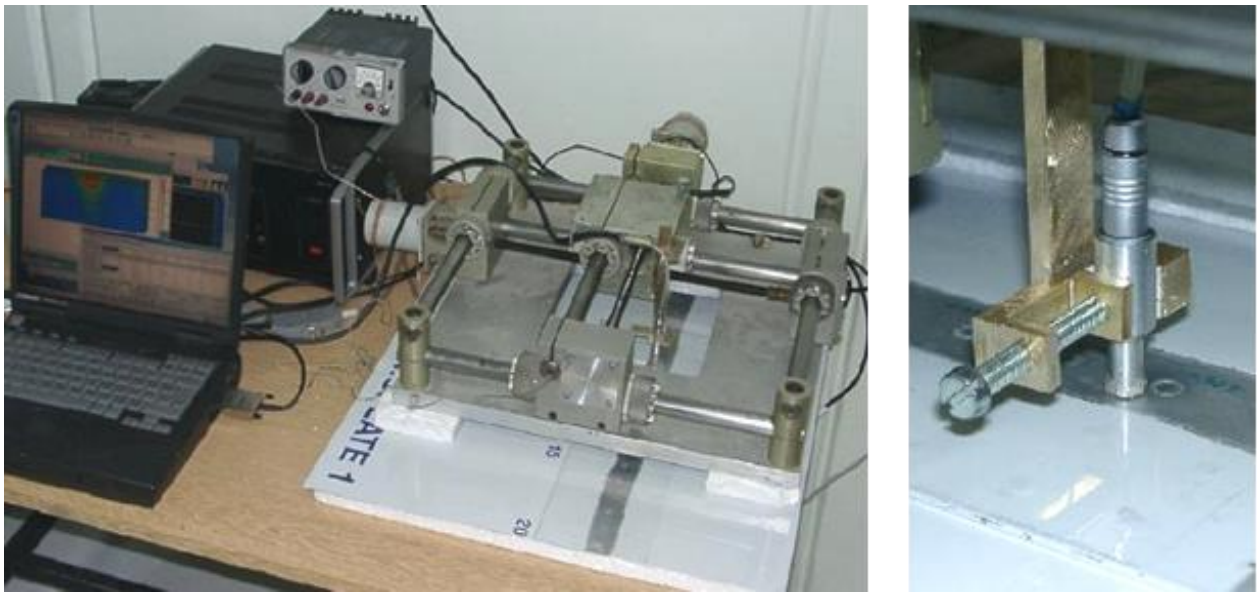

Fig. 3. Photos of Eddy current tomography setup with demo panel under investigation

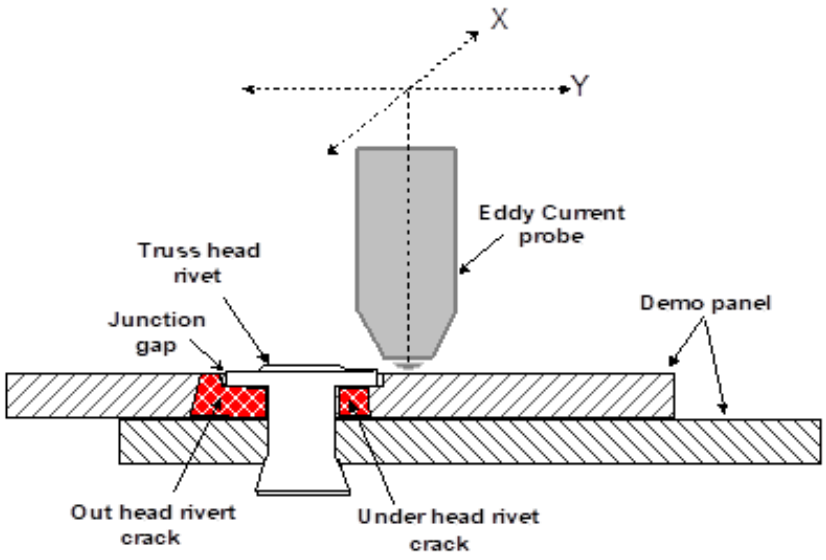

Fig. 4. Simplified schematic diagram of rivet junction

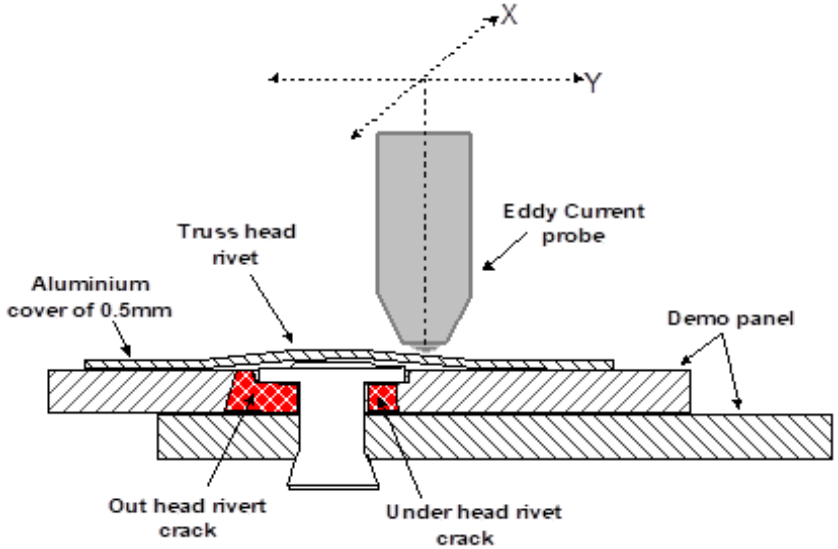

Fig. 5. Simplified schematic diagram of the covered rivet junction

ISSN 1814-4225 (print)
ISSN 2663-2012 (online)

Such subsurface condition of rivet junction is specified for eddy current tomography to reconstruct one as an obvious subsurface object. The open rivet junction with positioning number A12 has been tested. The procedure of the real scanning (the step-by-step depth slicing) is presented below in Fig. 6.

When 2-d scanning was finished, we obtained the horizontal slices for different depths. The reconstructed images of the A12 rivet junction for different depths are shown in Fig. 7. In the pictures presented below, we marked depths by symbol H.

As a result, the 3-D eddy current tomography image of the A12 rivet junction with crack is presented below in Fig. 8. As one can see, the cross-section has been found along the detected crack.

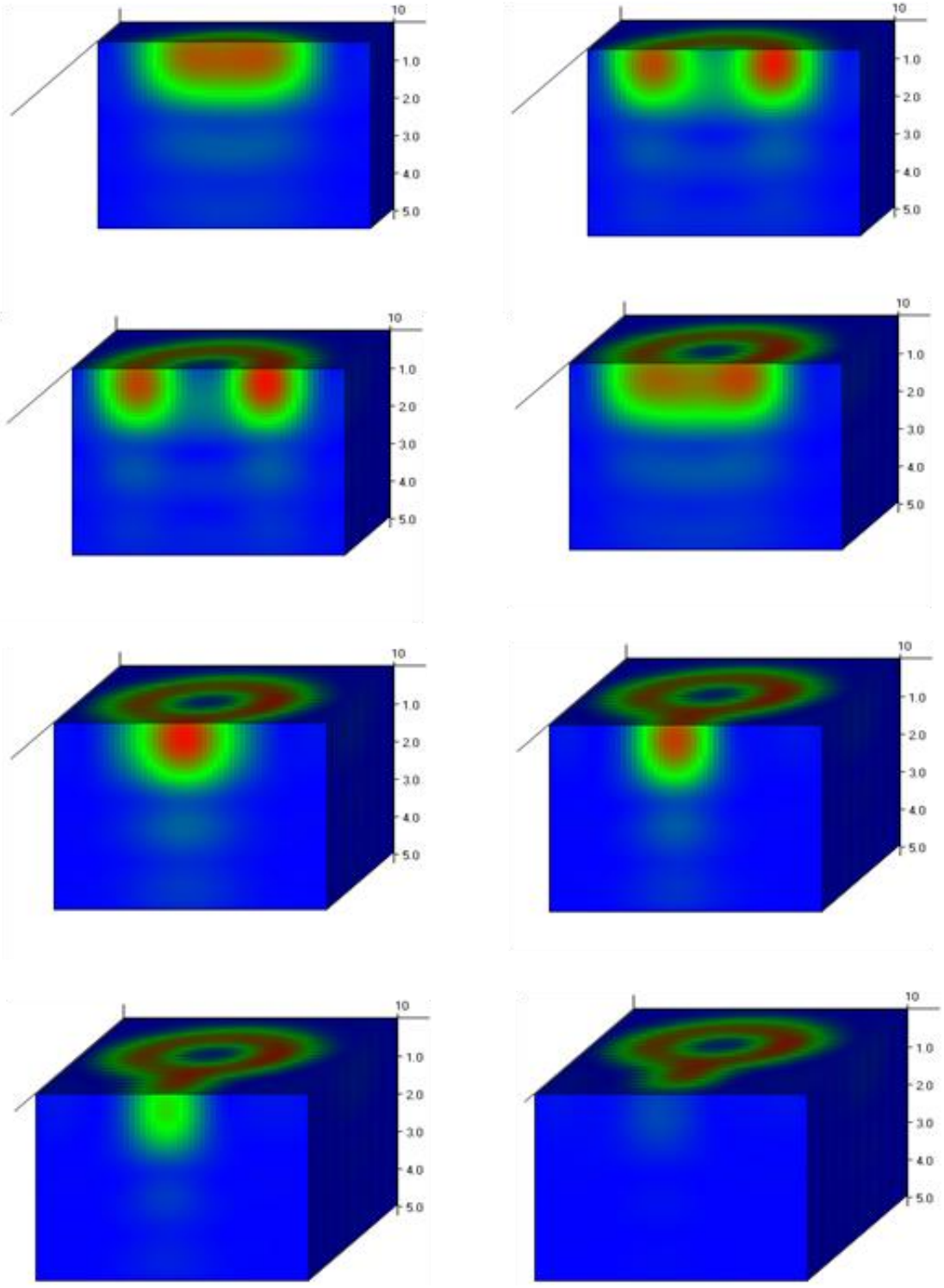

Fig. 6. Eddy current tomography imaging of rivet junction during the scanning

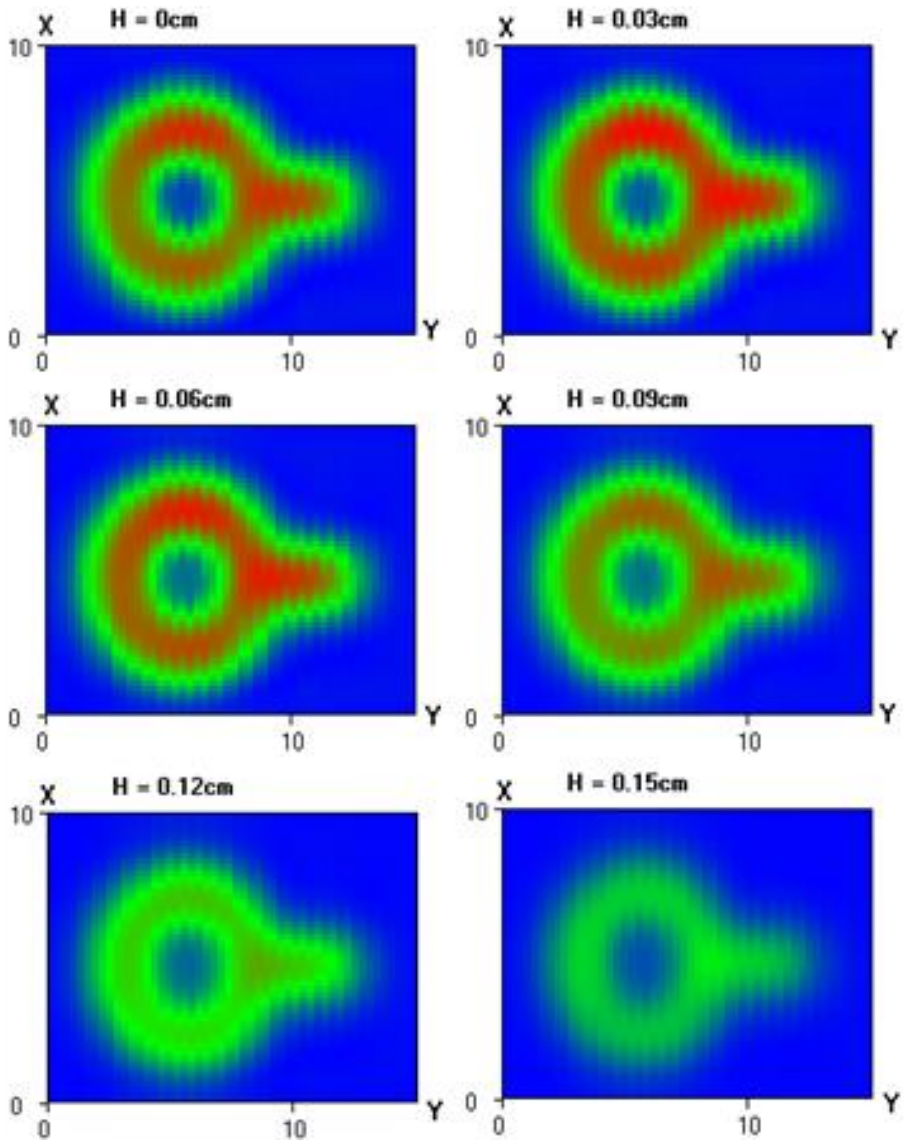

Fig. 7. Reconstructed images of A12 rivet junction for different depths

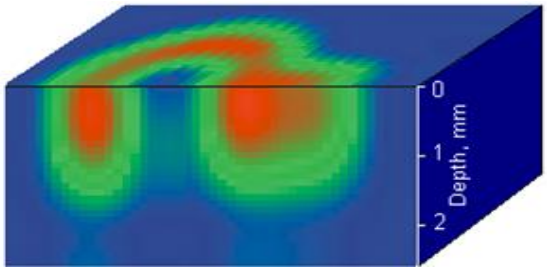

Fig. 8. 3-D cross-section along the crack that has been detected in A12 rivet junction

A similar procedure has been carried out for the A12 rivet junction, which is covered by the 0.5 mm thick aluminum alloy sheet (see Fig. 5). For the step-by-step scanning, the depth slicing is presented below in Fig. 9.

After finishing the 2-d scanning the horizontal slices for different depths can be obtained. The reconstructed images of covered A12 rivet junction for different depths are shown in Fig. 10. In our pictures, the depth is denoted as symbol H.

As a result, the 3-D eddy current tomography image of covered A12 rivet junction with crack is presented below in Fig. 11. As it is shown below, the cross-section has been found along the detected crack.

ISSN 1814-4225 (print)
ISSN 2663-2012 (online)

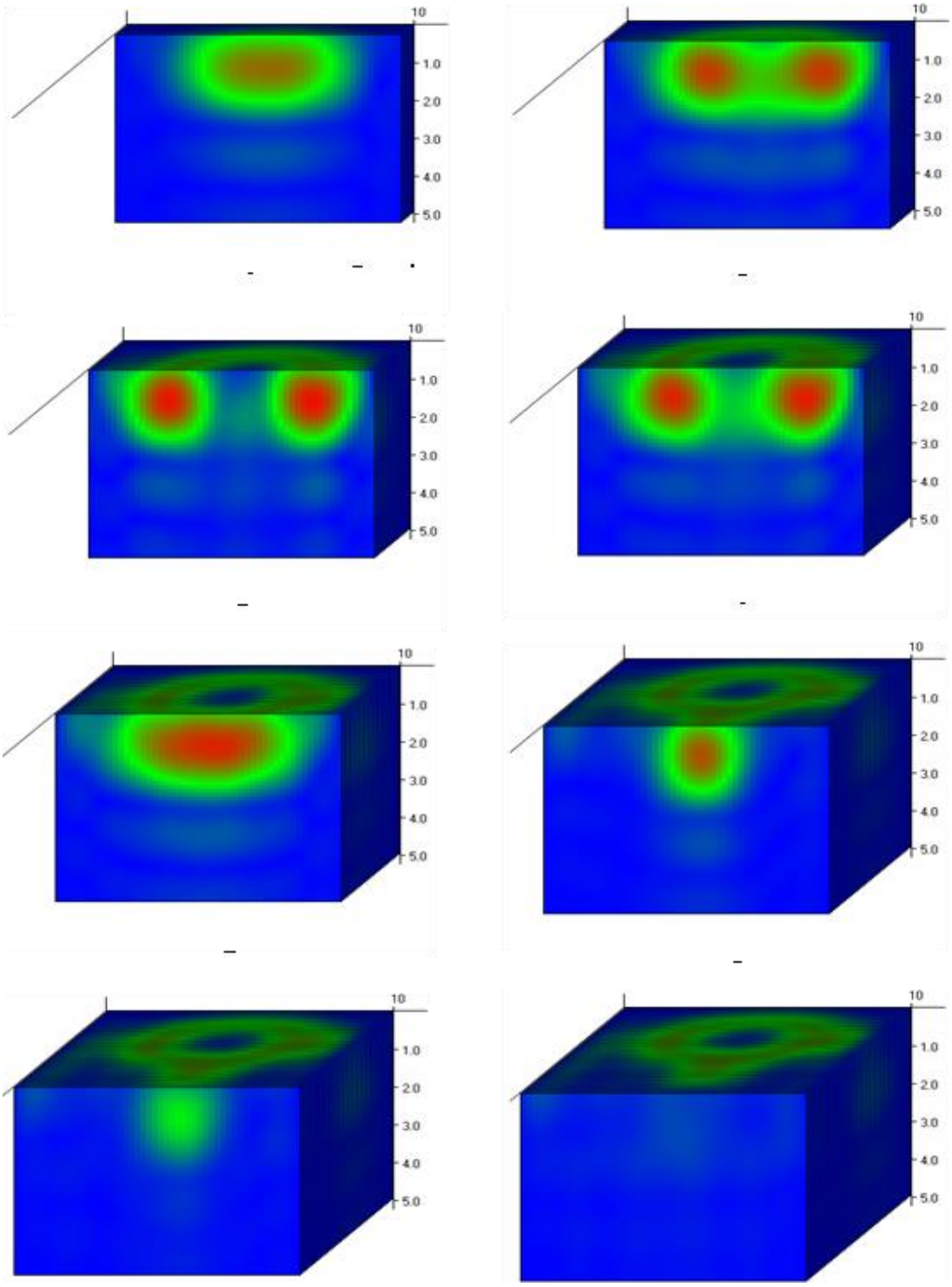

Fig. 9. Eddy current tomography imaging of the covered rivet junction during the scanning process

As it is seen from Fig. 11 the rivet junction is hidden under the surface at the depth of approximately 0.5 mm. Thus the eddy current tomography method reconstructed the covered A12 rivet junction as a visible subsurface object. Results of testing of another rivet junctions are presented in Fig. 12 – Fig. 19. Eddy current tomography reconstructed map of rivet junctions for 5…50 kHz frequency range is presented in Fig. 20. Images have been obtained at the depth of 0.9 mm. Similar measurements have been carried out for 100-1000 kHz frequency range using of appropriate eddy current absolute probe. Results of the measurements are shown in Fig. 21. The images have been obtained at the depth of 0.2 mm.

Also, it is possible to use imaging post-processing such as low-level's nulling and exclusive-or logical

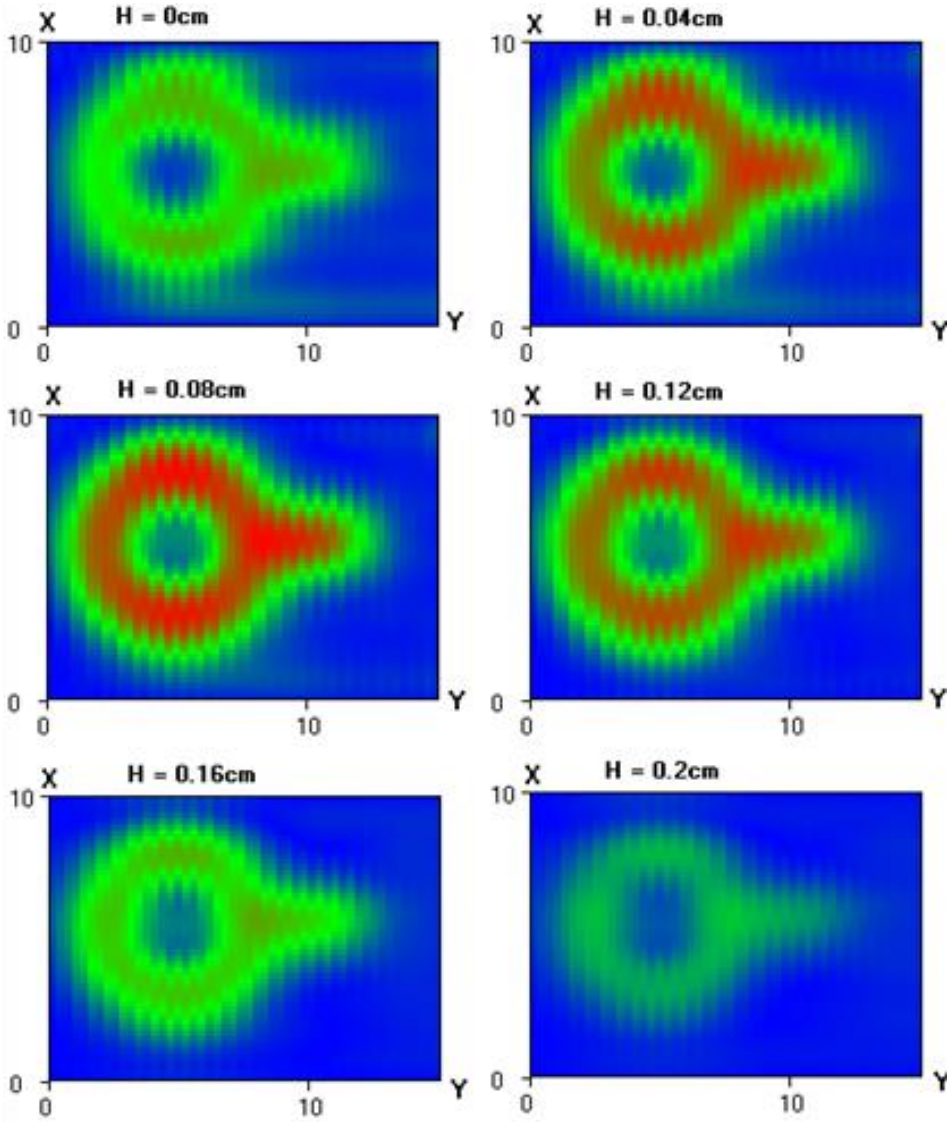

Fig. 10. Reconstructed images of covered A12 rivet junction for different depths

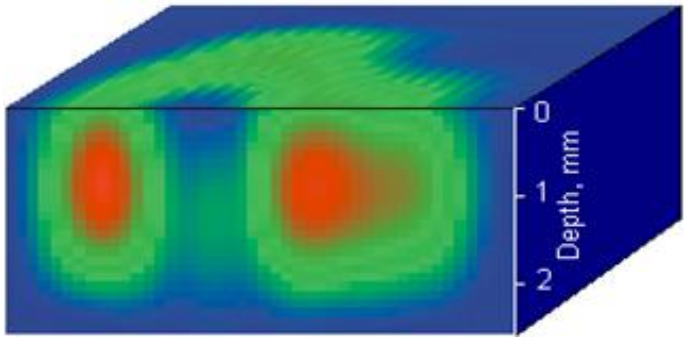

Fig. 11. 3-D cross-section along crack that has been detected for covered A12 rivet junction

computing. Low level's nulling is used for obtaining the outline of the rivet's junction. For example, the low level's nulling is shown in Fig. 22, where image rivet A15 without crack before (Fig. 22, a) and its outline after (Fig. 22, b) low level's nulling are presented. Following this way, the same processing has been applied to other rivets' junctions with possible cracks. The outlines are presented in Fig. 23. Results of applying an exclusive or logical function to the outlines are presented in Fig. 24. Outline image of rivet A15 (Fig. 22, b) is used as reference. Investigated images are outlines of rivets A9, A12 and A16.

ISSN 1814-4225 (print)
ISSN 2663-2012 (online)

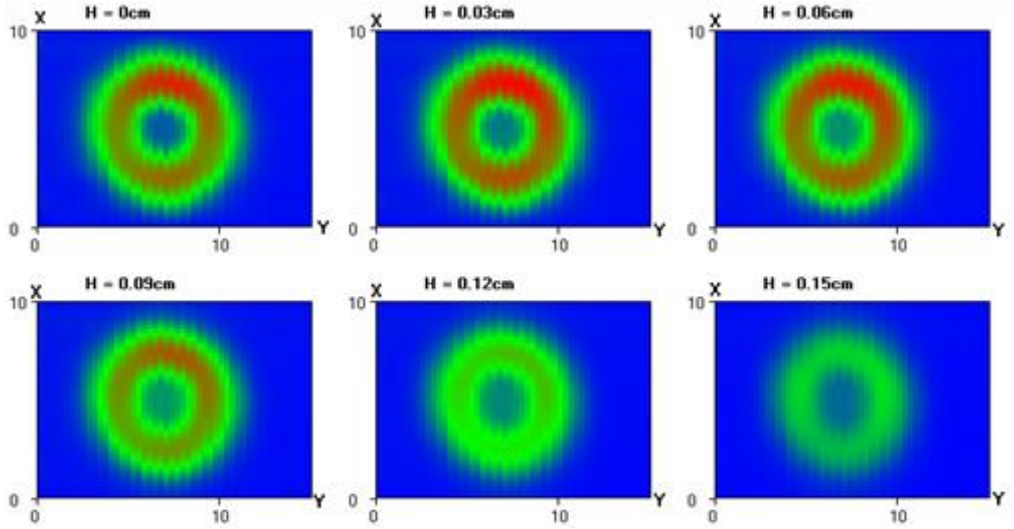

Fig. 12. Reconstructed images of A19 rivet junction for different depths. No cracks are here

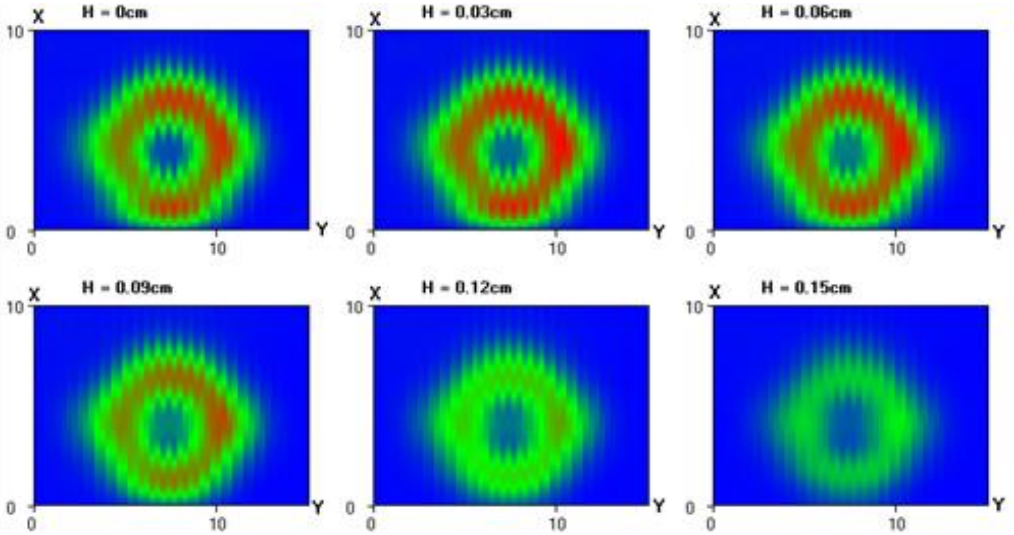

Fig. 13. Reconstructed images of A16 rivet junction for different depths. 2 cracks are here

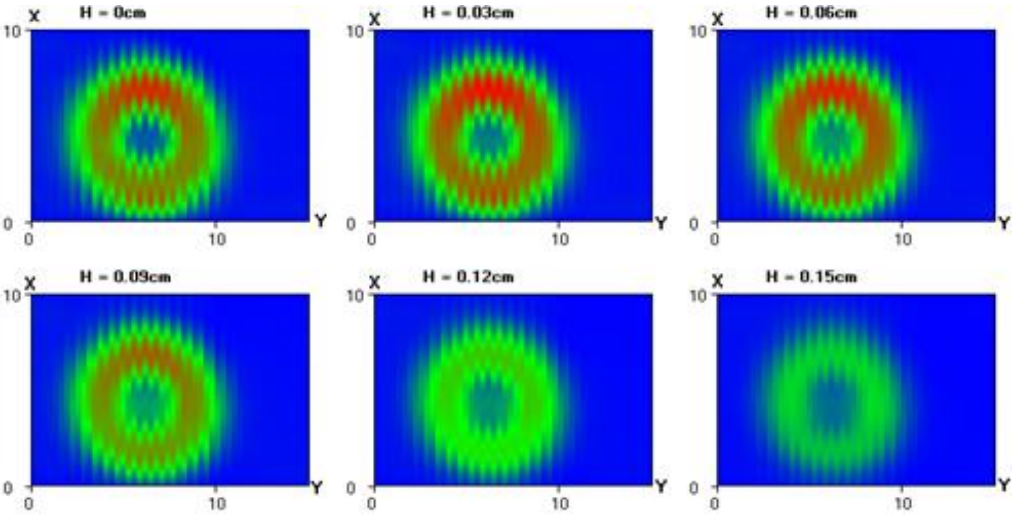

Fig. 14. Reconstructed images of A15 rivet junction for different depths. No cracks are here

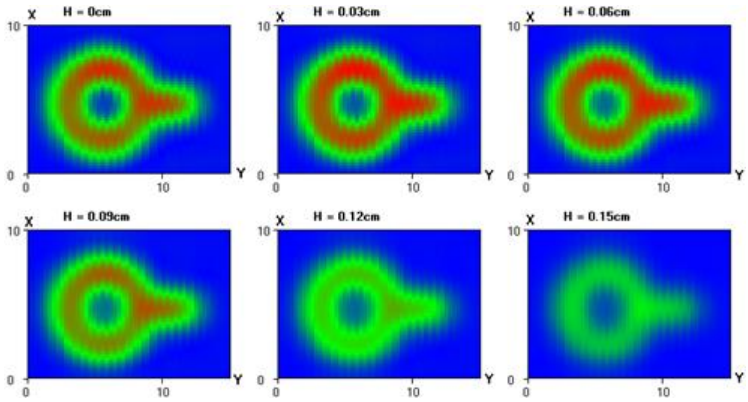

Fig. 15. Reconstructed images of A12 rivet junction for different depths. 1 cracks is here

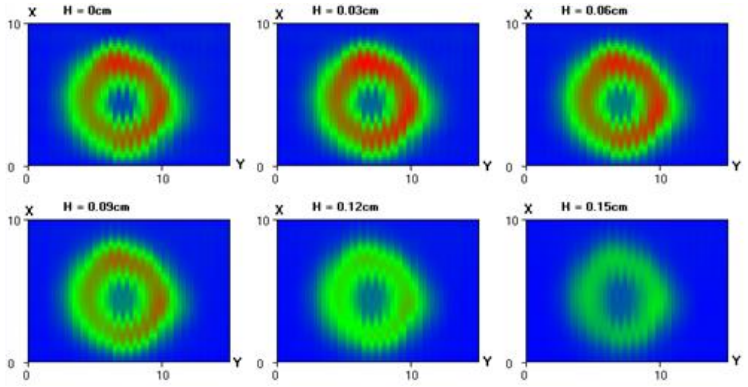

Fig. 16. Reconstructed images of A9 rivet junction for different depths. 1 cracks is here

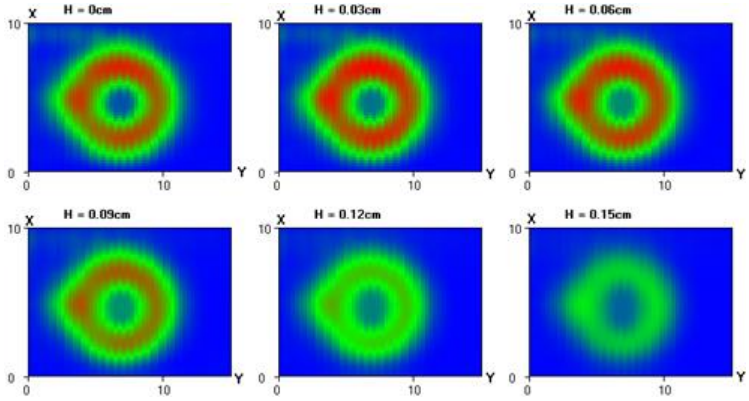

Fig. 17. Reconstructed images of A7 rivet junction for different depths. 1 crack

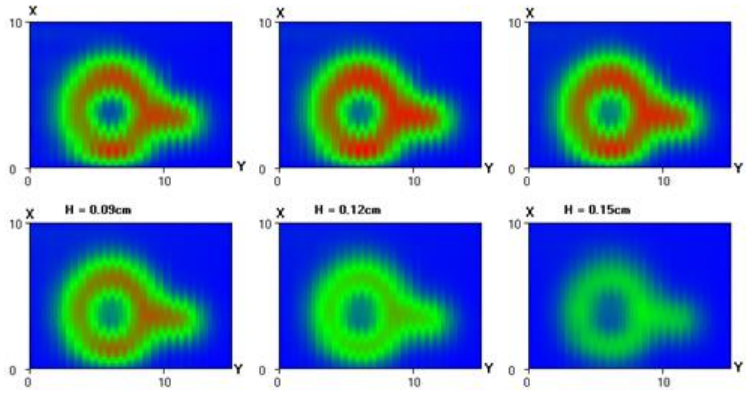

Fig. 18. Reconstructed images of A5 rivet junction for different depths. 1 crack

ISSN 1814-4225 (print)
ISSN 2663-2012 (online)

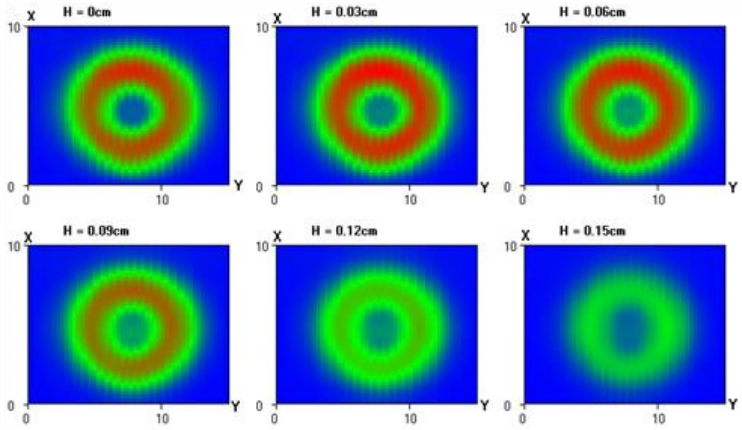

Fig. 19. Reconstructed images of A2 rivet junction for different depths. No cracks

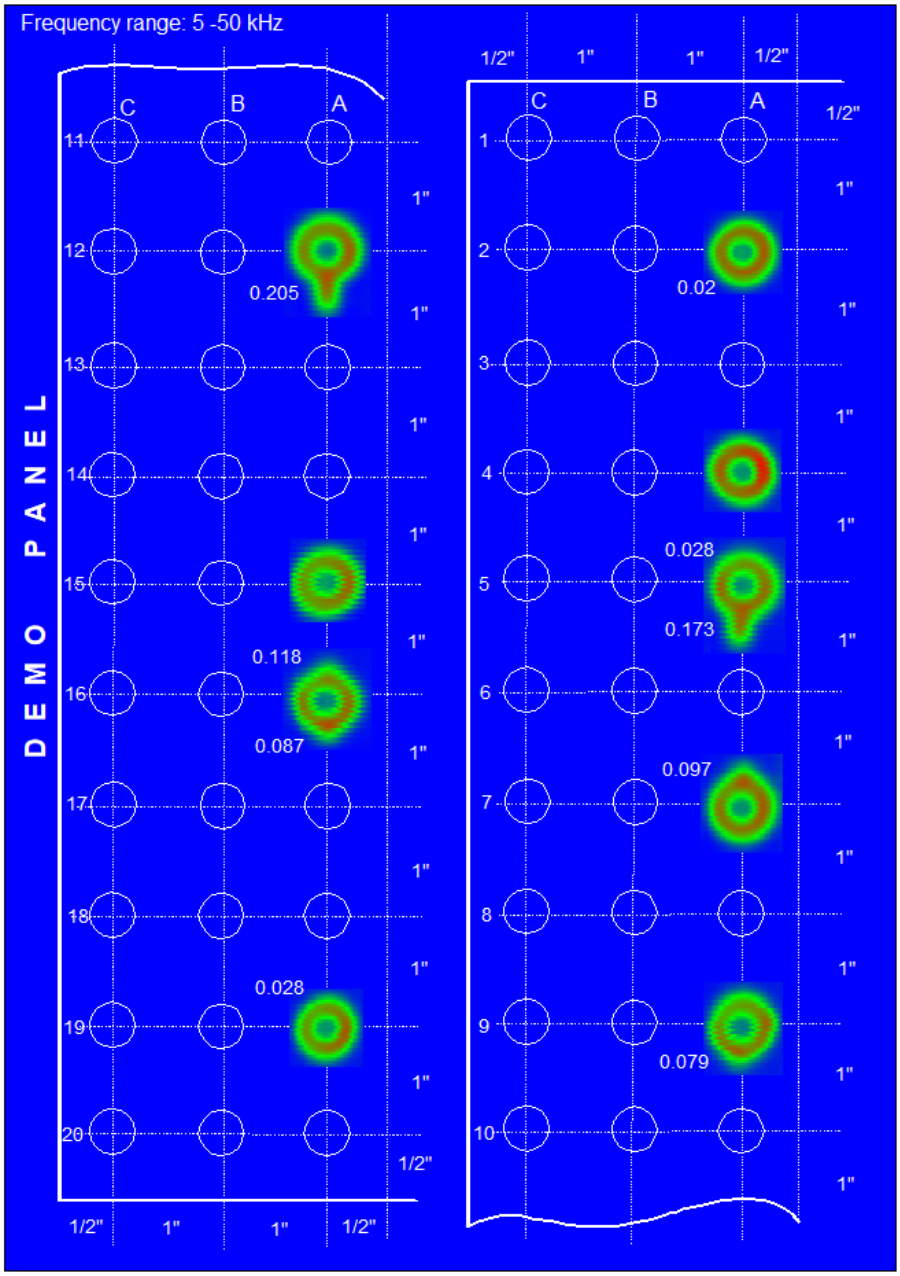

Fig. 20. Eddy current tomography reconstructed map of rivets for 5-50 kHz frequency range

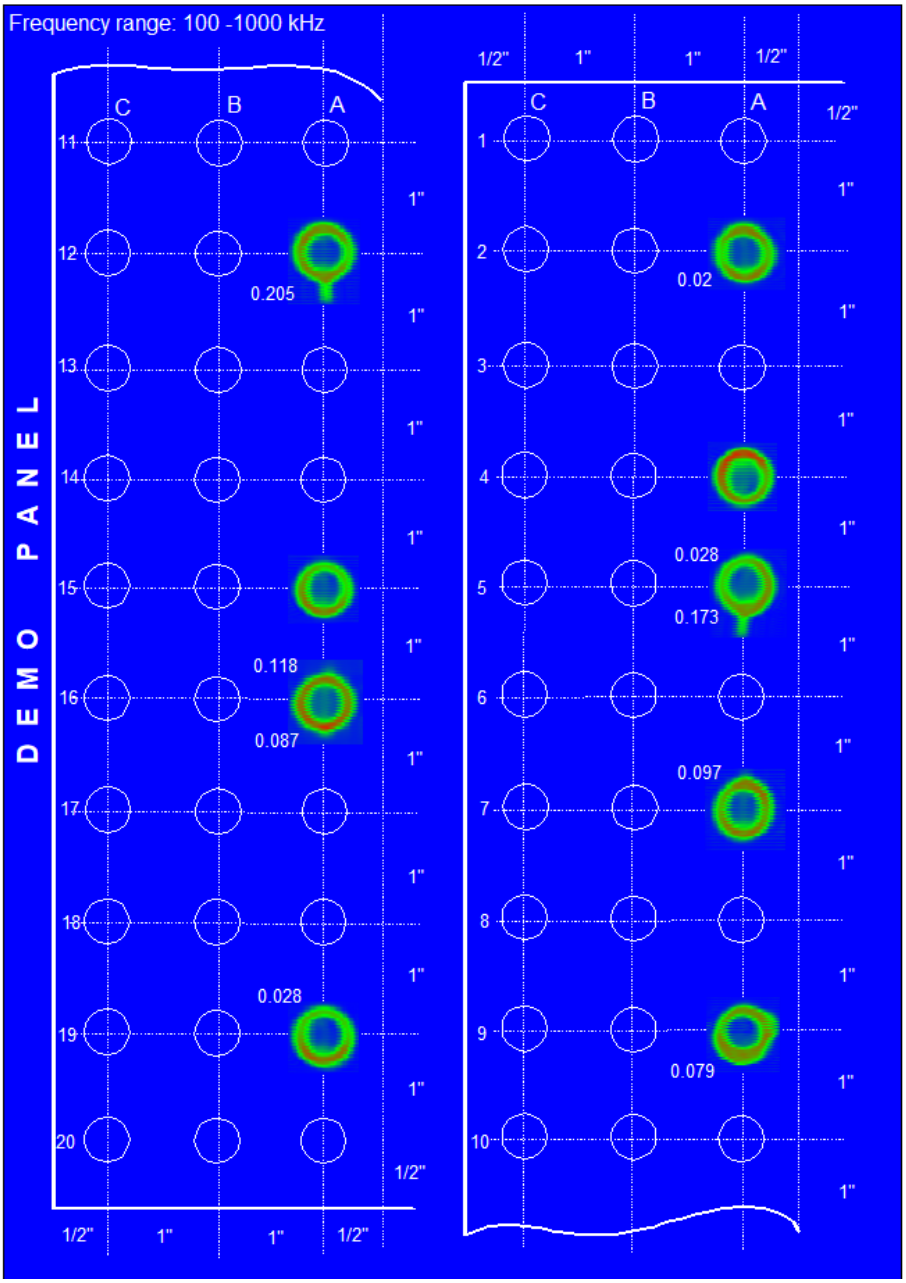

Fig. 21. Eddy current tomography reconstructed map of rivets for 100-1000 kHz frequency range

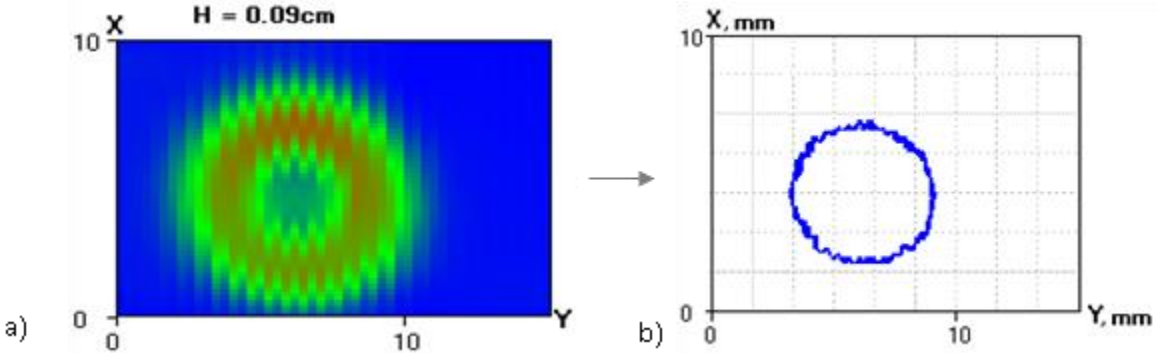

Fig. 22. Applying of low level's nulling for A15 rivet's junction: a – image before processing; b – outline as a result of low level's nulling

ISSN 1814-4225 (print)
ISSN 2663-2012 (online)

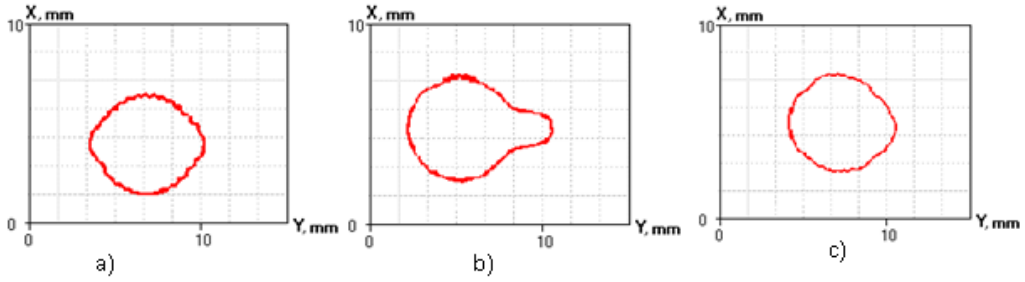

Fig. 23. After processing outlines of rivet's junctions with possibly cracks: a – A16; b – A12; c – A9

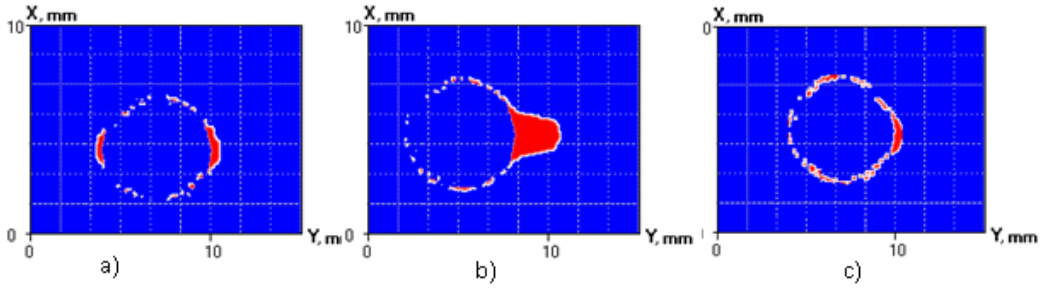

Fig. 24. Exclusive-or logical results of rivet's junctions with possibly cracks: a – A16; b – A12; c – A9

Using of low frequency range (50-50kHz) gives us more numbers of detected cracks that is a result of deeper penetration of the reactive field of the eddy current probe into metal. Using of higher frequency range (100-1000kHz) gives the better resolution. And determination of the optimal frequency range with satisfying resolution and penetration requires more detailed study of possibilities for detecting such kinds of cracks.

In conclusion, we would like to note one work that appeared quite recently, published by Ukrainian scientists [28], which, in our opinion, opens up a completely new direction associated with the inverse problems solution and which may have a serious impact on the development of methods for recovering the image of hidden defects.

Subsurface imaging by deep penetrating eddy current tomography

In this chapter new results of an experimental investigation on the object cross-section imaging by using the eddy current tomography technique are submitted for the case when the object is located far under the surface of the metal. The eddy current measurement setup contains a measuring unit with the eddy current probe MDF 1201(LEOTEST, Lviv) with penetration depth up to 8 mm.

The control of the subsurface areas form of the metal products is necessary for many technological processes. So, for example, in aerospace technology, it is very important to determine the presence of defects in aircrafts' multiple layer constructions. The same problems arise in chemical, power, and other industries, which are letting out the highly technological equipment. Defects and voids can be located far under a metal surface with residual depth up to 10 mm and more [27-29]. There is a problem with detection, identification, sizing, and imaging of such type inhomogeneities if the information about residual depth is absent.

Here it is offered to use the eddy current tomography technique [28, 29] for imaging of deep subsurface defects in metal.

Experimental results

The eddy current measurement setup consists of a measuring unit with the low-frequency multidifferential EC probe of MDF 1201 type [29, 30], PC Notebook, two-dimensional scanner, and the programmed scanner control block. The main features of the used EC probe for EC tomography application are good penetration in connection with high special resolution. Another interesting feature of this probe is a quasi-absolute signal response for prolonged defects used in these investigations. Fig. 25, Fig. 26 shows the scheme of conducted experiment with a slot.

In this experiment, two aluminum alloy plates by the thickness of 5 mm were placed on a base metal plate in such a way that the slot at a width of 0.3 mm remained between their flanks. Located in air EC probe scanned these plates and slot parallel to their surfaces along a direct line. The scanning length and step are 39.6 mm and 0.6 mm, correspondingly. The plate generatrixes are perpendicular to this direct line.

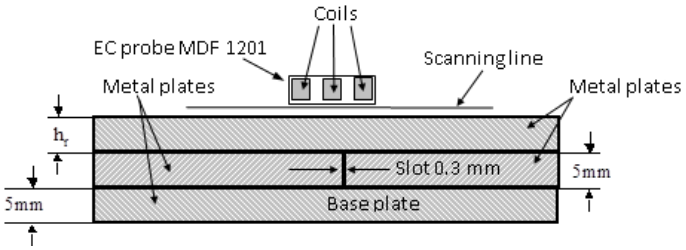

Fig. 25. Scheme of conducted experiment

Additional aluminum alloy plates of different thicknesses could be located from above plates with slots to simulate a defect disposed of in a metal depth with different residual depth hr. The above-described tomography method is used for the slot cross-section reconstruction in vertical to the metal surface plane (the image reconstruction plane) from the measured data. They have used 16 frequencies in the frequency band 0.9…10 kHz. Figure 26 illustrates reconstructed the structure cross-section image for residual depth hr=6.5 mm.

The rest of the experiments have been conducted free of defects and faulty rivets as well as with small holes located under the surface of a metal sample (aluminum alloy peace). The scheme of the experiment with rivets is presented in Fig. 27. In this study, the eddy current probe scans aluminum alloy sheets fastened by a rivet in the plane which is parallel to the sample surface (horizontal plane). Scanning lines are direct lines along X-axis. The image reconstruction planes are the vertical planes parallel to the XOZ plane. The set of the sample vertical cross-section images has been obtained by the additional scanning along Y-axis. The scanning area along X and Y-axes is 20 x 20 mm, the scanning length and step along X-axis is 14.7 mm and 0.3 mm, the scanning length and step along Y-axis is 19.6 mm and 0.4 mm. They have used 16 frequencies in the frequency band 1.2…0.5 kHz. The obtained sample vertical cross-section images allow building the sample cross-section images in horizontal planes (horizontal slices) for the depth range.

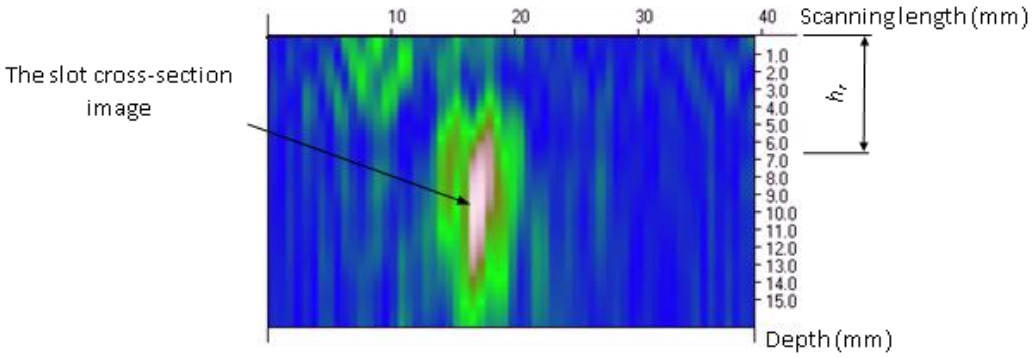

Fig. 26. Image reconstructed by using eddy current tomography for the structure cross-section shown in Fig.1

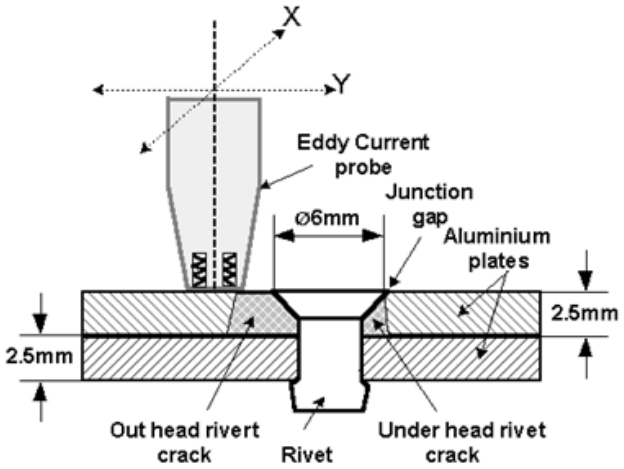

Fig. 27. Scheme of the experiment with rivets

ISSN 1814-4225 (print)
ISSN 2663-2012 (online)

Some experimental results are presented in Fig. 28 and Fig. 29. Figure 28 illustrates horizontal slices of the studied rivet at different depths H= 0, 1, 2, 2.5, 3, and 4 mm in the case when the rivet crack is absent.

Horizontal slices for the same depths in the case of the out head rivet crack are shown in Fig. 29. One can see significant disagreement between the horizontal slices structures in Fig. 4 and Fig. 5. The crack presence leads to perturbation of the eddy currents symmetrical structure existing around the defect-free rivet. As a result, the eddy current amplitude distribution on horizontal slices in Fig. 29 is asymmetric. One of four spots is absent and it is possible to observe the crack trail on the place of the missing spot.

An experiment with holes has been conducted on the same scheme as in the case of the slot studying (Fig. 25). But two plates composing the slot were not used. Instead of it, the small hole has been scooped in the base plate at a right angle to its surfaces. The diameter of the hole is 0.8 mm and its depth size is 1.2 mm. The base plate thickness is 10.0 mm. The base plate was covered by aluminium alloy sheet of thickness h_r from open side of hole for modelling of small cylindrical defect located at residual depth h_r in the metal. The eddy current probe scans the structure above aluminium alloy sheet around the hole as shown in Fig. 27. The scanning length and step along X-axis are 9.9 mm and 0.3 mm, the scanning length and step along Y-axis are 9.9 mm and 0.4 mm. They were used 16 frequencies in the frequency band 2.0-20.0 kHz. The horizontal slices of the metal structure containing the hole have been built for different depth H = 0.0, 0.5, 1.0, 1.5, 2.0 and 2.5 mm at h_r=0.7 mm. One can see that pictures in Fig. 30 have at $H \cong h_r$ best contrast and brightness.

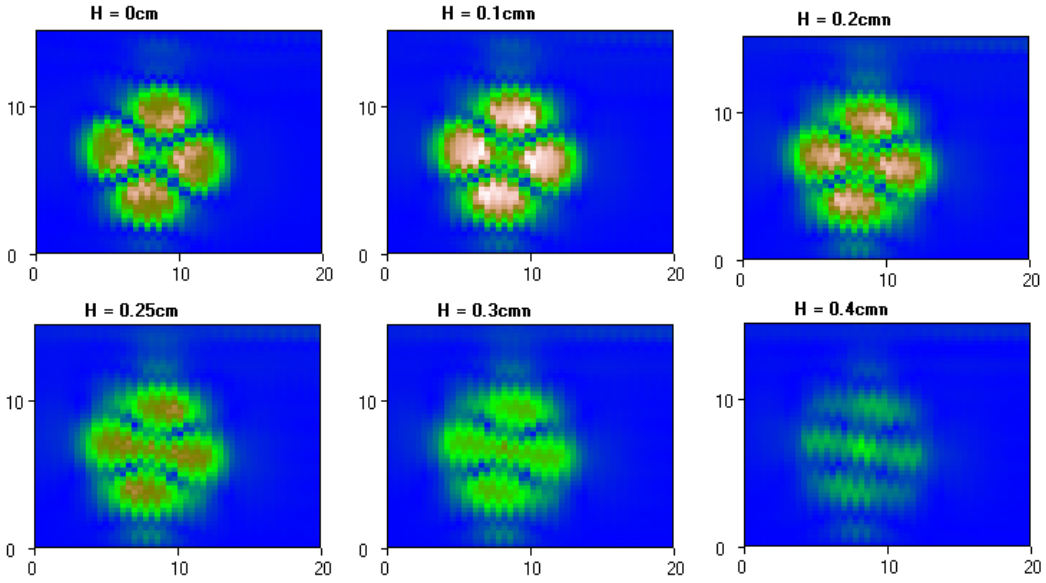

Fig. 28. Horizontal slices of the studied rivet at different depth in the case when the rivet cracks are absent

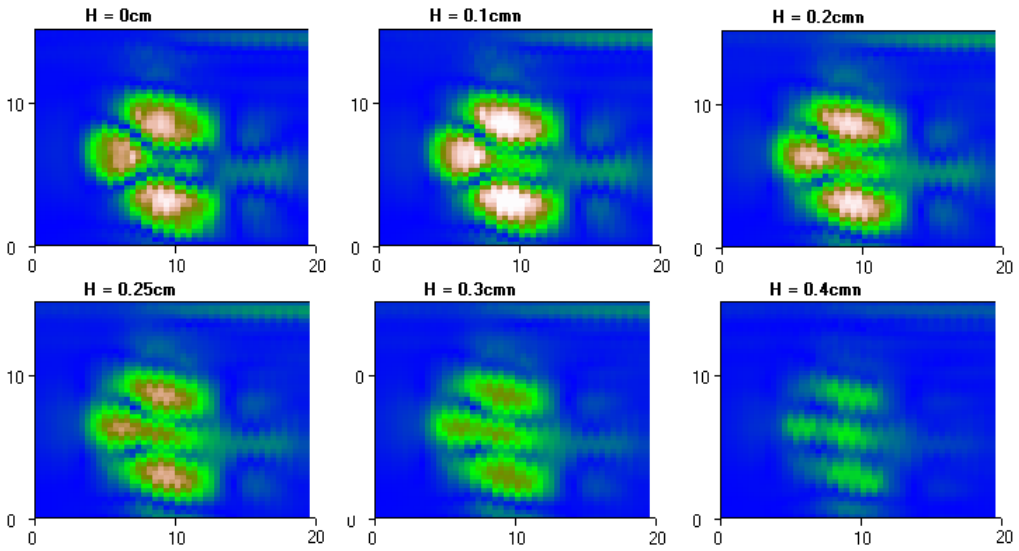

Fig. 29. Horizontal slices of the studied rivet at different depth in the case of the rivet crack presence

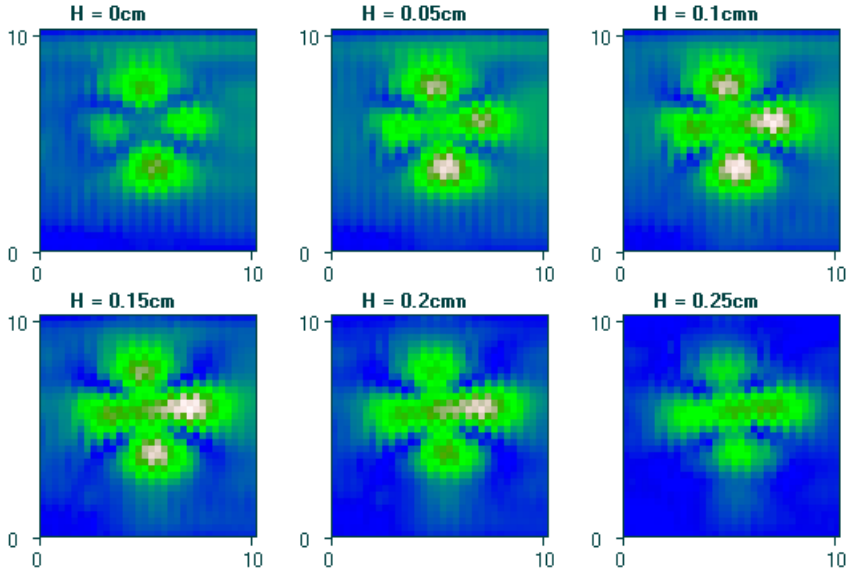

Fig. 30. Horizontal slices of the studied hole (drilling) at different depth in the case of the rivet crack presence

The measurement setup and technology developed for the eddy current tomography imaging have been optimized for portability. This version of the system contains:

- Desktop or portable computer equipped with data acquisition board (DAQ-board);
- Small-sized and light-weighted vector measuring unit (1kHz-10MHz working frequency band);
- Eddy current probe;
- Scanning control block.

Thus, the experiments were carried out to confirm the possibility of deep detection of defects in metals and the imaging of deep subsurface defects in metal.

Conclusions

In practice by the method of eddy current tomography, it is received the 3D object images in conducting environments with the super-resolution. It is shown that the method of near (evanescent) field tomography allows to receive obtained images of the subsurface defects in highly conducting environments with the resolution in shares millimeters on the frequency a few kHz. The considered method of near-field subsurface tomography has allowed receiving high-quality images of real subsurface objects. The received results can find application for the control of dangerous cracks in avionics etc.

Future research directions

The results of the eddy current tomography presented here show a significant potential of the capabilities of this method, in particular, for non-destructive testing in the aviation industry. One of the prospective directions of eddy current tomography development is spatial resolution improvement. The next stage of our program in the framework of the creation of high-resolution tomographs will be the transition to the GHz frequencies range.

It should be noted that a significant contribution to the development of the mathematical aspects of the method under consideration was made with S. Gavrilov.

References (GOST 7.1:2006)

1. Review of Progress in Quantitative nondestructive evaluation [Text] / D. O. Thompson, D. E. Chimenti (Editors). – NY : Plenum Press, 1991. – Vol. 10A/B.

2. Bernieri, A. Eddy current testing probe based on double-coil excitation and GMR sensor [Text] / A. Bernieri, L. Ferrigno, M. Laracca and A. Rasile // IEEE Trans. Instrum. Meas. – 2019. – Vol. MAG-68. – P. 1533–1542.

3. Lean, M. H. Application of Boundary Integral Equation Methods to electromagnetics. The Hybrid Finite Element-Boundary Element method in electromagnetics [Text] / M. H. Lean // IEEE Trans. on Magnetics. – 1985. – Vol. MAG-21, no. 5. – P. 1823–1828.

4. Demonstration of model-based inversion of electromagnetic signals for crack characterization [Text] / E. B. Shell, J. C. Aldrin, H. A. Sabbagh, E. Sabbagh, R. K. Murphy, S. Mazdiyasni, E. A. Lindgren // 41st Annual Review of Progress in Quantitative Nondestructive Evaluation. – 2015. – Vol. MAG-34. – P. 484–493.

5. Uemura, C. Estimating POD of a screening technique for cracks about ferrous fasteners without fastener [Text] / C. Uemura, P. Underhill, T. Krause // NDT & E International. – 2019. – Vol. MAG-107. – P. 1–9.

6. Kent, K. R. The use of Null Field Integral Equations in Magnetic-Field Problems [Text] / K. R. Davey, Y. Kanai // IEEE Trans. on Magnetics. – 1986. –

ISSN 1814-4225 (print)
ISSN 2663-2012 (online)

Vol. MAG-22, no. 4. – P. 292-298.

7. Ishibashi, K. Nonlinear eddy current analysis by volume integral equation method [Text] / K. Ishibashi // IEEE Trans. on Magnetics. – 1987. – Vol. MAG-23, no. 5. – P. 3038-3040.

8. Єремеєв, О. І. Комбінована метрика візуальної якості зображень дистанційного зондування на основі нейронної мережі [Текст] / О. І. Єремеєв, В. В. Лукін, К. Окарма // Радіоелектронні і комп'ютерні системи. – 2020. – № 4(96). – С. 4-15. DOI: 10.32620/reks.2020.4.01.

9. Uchanin, V. Detection of cracks in ferrous steel structures: new innovative eddy current techniques [Text] / V. Uchanin, G. Nardoni // Procedia Structural Integrity (ESIS). – 2019. – Vol. MAG-16. – P. 198-204.

10. Ross, S. Application of a Diffusion-to-Wave transformation for Inverting Eddy Current Nondestructive Evaluation Data [Text] / S. Ross, M. Lusk, W. Lord // IEEE Trans. on Magnetics. – 1996. – Vol. MAG-32, no. 2. – P. 535-546.

11. Ishibashi, K. Eddy Current Analysis by Integral Equation Method Utilizing Loop Electric and Surface Magnetic Currents as Unknowns [Text] / K. Ishibashi // IEEE Trans. on Magnetics. – 1998. – Vol. MAG-34, no. 5. – P. 2585–2588.

12. Egorov, A. V. Inspection of aluminum alloys by a multi-frequency eddy current method [Text] / A. V. Egorov, V. V. Polyakov, D. S. Salita, E. A. Kolubaev, S. G. Psakhie, A. G. Chernyavskii, I. V. Vorobei // Defence Technology. – 2015. – Vol. MAG-11, no. 2. – P. 99-103.

13. Norton, S. J. Theory of eddy current inversion [Text] / S. J. Norton, J. R. Bowler // J. Appl. Phys. – 1993. – Vol. 73(2). – P. 501-512.

14. Enokizono, M. Numerical Approach for ECT by using Boundary Element Method with Laplace Transform [Text] / M. Enokizono, T. Todaka, K. Shibao // IEEE Trans. on Magnetics. – 1997. – Vol. MAG-33, no. 2. – P. 2135-2138.

15. Tytko, G. E-Cored Coil With a Circular Air Gap Inside the Core Column Used in Eddy Current Testing [Text] / G. Tytko, L. Dziczkowski // IEEE Trans. on Magnetics. – 2015. – Vol. MAG-51, no. 9. – P. 1-4.

16. Rekanos, I. T. Electromagnetic Field Inversion Using the Quickprop method [Text] / I. T. Rekanos, T. D. Tsiboukis // IEEE Trans. on Magnetics. – 1997. – Vol. MAG-33, no. 2. – P. 1872-1875.

17. Методика определения поля обнаружения беспилотных летательных аппаратов наземным наблюдателем [Текст] / С. К. Абрамов, В. В. Абрамова, К. Д. Абрамов, В. В. Лукин, В. В. Бондарь, И. В. Калужинов // Радіоелектронні і комп'ютерні системи. – 2020. – № 3(95). – С. 36-42. DOI: 10.32620/reks.2020.3.04.

18. Alatawneh, N. Low-Frequency Eddy-Current Testing for Detection of Subsurface Cracks in CF-188 Stub Flange [Text] / N. Alatawneh, P. R. Underhill, T. W. Krause // IEEE Sens. J. – 2018. – Vol. MAG-18. – P. 1568 – 1575.

19. Abdou, A. A Method for Crack Detection in Multilayer Riveted Structures [Text] / A. Abdou, O. A. Safer, T. Bouchala, A. Bendaikha, B. Abdelhadi, A. Guettafi, A. Benoudjit // Instrumentation Mesure Metrologie. – 2019. – Vol. MAG-18. – P. 485-490.

20. Ash, E. A. Super-resolution aperture scanning microscope [Text] / E. A. Ash, G. Nicholls // Nature. – 1972. – Vol. 237. – P. 510-512.

21. Nozokido, T. Scanning Near-Field Millimeter-Wave Microscopy using a Metal Slit as a Scanning Probe [Text] / Tatsuo Nozokido, Jongsuck Bae, Koji Mizuno // IEEE Trans. Microwave Theory Tech. – 2001. – Vol. 49, no. 3. – P. 491-498.

22. The Millimeter wave tomography application for the subsurface imaging [Text] / A. A. Vertiy, S. P.Gavrilov, I. V. Voynovskyy, V. N. Stepanyuk, Sunullah Ozbek // International Journal of Infrared and Millimeter Waves. – 2002. – Vol. 23, no. 10. – P. 1413-1444.

23. Chommeloux, L. Electromagnetic Modelling for Microwave Imaging of Cylindrical Buried Inhomogeneities [Text] / L. Chommeloux, Ch. Pichot, J.-Ch. Bolomey // IEEE Trans. Microwave Theory Tech. – 1986. – Vol. MTT–34, no. 10. – P. 1064 – 1076.

24. Vertiy, A. A. Modelling of Microwave Images of Buried Cylindrical Objects [Text] / A. A. Vertiy, S. P. Gavrilov // International Journal of Infrared and Millimetre Waves. – 1998. – Vol. 19, no. 9. – P. 1201-1220.

25. Smith, Glenn S. Directive Properties of Antennas for Transmission into a Material Half-Space [Text] / Glenn S. Smith // IEEE Trans. Antennas and Propagation. – 1984. – Vol. AP-32, no. 3. – P. 232-246.

26. Exact Solutions of Electromagnetic Fields in Both Near and Far Zones Radiated by Thin Circular-Loop Antennas: A General Representation [Text] / Le-Wei Li, Mook-Seng Leong, Pang-Shyan Kooi, Tat-Soon Yeo // IEEE Trans. Antennas and Propagation. – 1997. – Vol. 45, no. 12. – P. 1741-1748.

27. Ahmet, S. Subsurface Sensing [Text] / S. Ahmet, A. Turk, Koksal Hocaoglu, A. Vertiy. – John Wiley & Sons, Inc., 2011. – 960 p..

28. Melezhik, P. N. Numerical-analytical method for determining the dielectric constant of 1d inhomogeneous plate in a waveguide. [Text] / P. N. Melezhik, V. Y. Morozov, A. Y. Poyedinchuk, S. V. Mizrakhy, P. K. Nesterov, A. A. Vertiy // IET Microwaves, Antennas & Propagation. – 2020. – Vol. MAG–14. – P. 1878-1885.

29. Mook, G. Deep Penetrating Eddy Currents and Probes [Text] / G. Mook, J. Hesse, V. Uchanin // Materials Testing. – 2007. – Vol. MAG–49, no. 5. – P. 258-264.

30. Uchanin, V. Detection of the fatigue cracks initiated near the rivet holes by eddy current inspection techniques [Text] / V. Uchanin // Transactions on Aerospace Research. – 2020. – no. 1 (258). – P. 47-58.

References (BSI)

1. Thompson, D. O., Chimenti, D. E. (Editors). *Review of Progress in Quantitative nondestructive evaluation*, 1991, vol. 10A/B, New York, Plenum Press Publ.

2. Bernieri, A., Ferrigno, L., Laracca, M., Rasile, A. Eddy current testing probe based on dou-ble-coil excitation and GMR sensor. *IEEE Trans. Instrum. Meas*, 2019, vol. 68, pp. 1533-1542.

3. Meng, H. Lean Application of Boundary Integral Equation Methods to electromagnetics. “The Hybrid Finite Element-Boundary Element method in electromagnetics. *IEEE Trans. on Magnetics*, 1985, vol. 21, no. 5, pp. 1823-1828.

4. Shell, E. B., Aldrin, J. C., Sabbagh, H. A., Sabbagh, E., Murphy, R. K., Mazdiyasni, S., Lindgren, E. A. Demonstration of model-based inversion of electromagnetic signals for crack characterization. *41st Annual Review of Progress in Quantitative Non-destructive Evaluation*, 2015, vol. 34, pp. 484–493.

5. Uemura, C., Underhill, P., Krause, T. Estimating POD of a screening technique for cracks about ferrous fasteners without fastener. *NDT & E International*, 2019, vol. 107, pp. 1–9.

6. Kent, K. R., Kanai, Y. The use of Null Field Integral Equations in Magnetic-Field Problems. *IEEE Trans. on Magnetics*, 1986, vol. 22, no. 4, pp. 292-298.

7. Ishibashi, K. Nonlinear eddy current analysis by volume integral equation method. *IEEE Trans. on Magnetics*, 1987, vol. MAG-23, no. 5, pp. 3038-3040.

8. Ieremeiev, O., Lukin, V., Okarma, K. Kombinovana metryka vizual'noyi yakosti zobrazhen' dystantsiynoho zonduvannya na osnovi neyronnoyi merezhi [Combined visual quality metric of remote sensing images based on neural network]. *Radioelektronni i komp'uterni sistemi – Radioelectronic and computer systems,* 2020, no. 4(96), pp. 4-15. DOI: 10.32620/reks.2020.4.01.

9. Uchanin, V., Nardoni, G. Detection of cracks in ferrous steel structures: new innovative eddy current techniques. *Procedia Structural Integrity (ESIS)*, 2019, vol. 16, pp. 198-204.

10. Ross, S., Lusk, M., Lord, W. Application of a Diffusion-to-Wave transformation for Inverting Eddy Current Nondestructive Evaluation Data. *IEEE Trans. on Magnetics*, 1996, vol. 32, no. 2, pp. 535-546.

11. Ishibashi, K. Eddy Current Analysis by Integral Equation Method Utilizing Loop Electric and Surface Magnetic Currents as Unknowns. *IEEE Trans. on Magnetics*, 1998, vol. 34, no. 5, pp. 2585–2588.

12. Egorov, A. V., Polyakov, V. V., Salita, D. S., Kolubaev, E. A., Psakhie, S. G., Chernyavskii, A. G., Vorobei, I. V. Inspection of aluminum alloys by a multifrequency eddy current method. *Defence Technology*, 2015, vol. 11, no. 2, pp. 99-103.

13. Norton, S. J., Bowler, J. R. Theory of eddy current inversion. *J. Appl. Phys.*, 1993, vol. 73(2), pp. 501-512.

14. Enokizono, M., Todaka, T., Shibao K. Numerical Approach for ECT by using Boundary Element Method with Laplace Transform. *IEEE Trans. On Magnetics*, 1997, vol. 33, no. 2, pp. 2135-2138.

15. Tytko, G., Dziczkowski, L., E-Cored Coil With a Circular Air Gap Inside the Core Column Used in Eddy Current Testing. *IEEE Trans. on Magnetics*, 2015, vol. 51, no. 9, pp. 1-4.

16. Rekanos, I. T., Tsiboukis, T. D. Electromagnetic Field Inversion Using the Quickprop method. *IEEE Trans. on Magnetics*, 1997, vol. 33, no. 2, pp. 1872-1875.

17. Abramov, S. K., Abramova, V. V., Abramov, K. D., Lukin, V. V., Bondar, V. V., Kaluzhinov, I. V. Metodika opredelenija polja obnaruzhenija bespilotnyh letatel'n-yh apparatov nazemnym nabljudatelem [Technique of detection field estimating for unmanned aerial vehicles by a ground observer]. *Radioelektronni i komp'uterni sistemi – Radioelectronic and computer systems,* 2020, no. 3(95), pp. 36-42. DOI: 10.32620/reks.2020.3.04.

18. Alatawneh, N., Underhill, P. R., Krause, T. W. Low-Frequency Eddy-Current Testing for Detection of Subsurface Cracks in CF-188 Stub Flange. *IEEE Sens. J*, 2018, vol. 18, pp. 1568-1575.

19. Abdou, A. A., Safer, O. A., Bouchala, T., Bendaikha, A., Abdelhadi, B., Guettafi, A., Benoudjit A. Method for Crack Detection in Multilayer Riveted Structures. *Instrumentation Mesure Metrologie,* 2019, vol. 18, pp. 485-490.

20. Ash, E. A., Nicholls, G. Super-resolution aperture scanning microscope. *Nature*, 1972, vol. 237, pp. 510-512.

21. Nozokido, T., Bae, J., Mizuno, K. Scanning Near-Field Millimeter-Wave Microscopy using a Metal Slit as a Scanning Probe. *IEEE Trans. Microwave Theory Tech.*, 2001, vol. 49, no. 3, pp. 491-498.

22. Vertiy, A., Gavrilov, S. P., Voynovskyy, I. V., Stepanyuk, V. N., Ozbek, Sunul-lah. The Millimeter wave tomography application for the subsurface imaging. *International Journal of Infrared and Millimeter Waves*, 2002, vol. 23, no. 10, pp. 1413-1444.

23. Chommeloux, L., Pichot, Ch., Bolomey, J.-Ch. Electromagnetic Modelling for Microwave Imaging of Cylindrical Buried Inhomogeneities. *IEEE Trans. Microwave Theory Tech.*, 1986, vol. MTT–34, no. 10, pp. 1064-1076.

24. Vertiy, A. A., Gavrilov, S. P. Modelling of Microwave Images of Buried Cylindrical Objects. *International Journal of Infrared and Millimetre Waves*, 1998, vol. 19, no. 9, pp. 1201-1220.

25. Smith, G. S. Directive Properties of Antennas for Transmission into a Material Half-Space. *IEEE Trans. Antennas and Propagation*, 1984, vol. AP-32, no. 3, pp. 232-246.

26. Li, Le-Wei, Leong, Mook-Seng, Kooi, Pang-Shyan, Yeo, Tat-Soon Exact Solutions of Electromagnetic Fields in Both Near and Far Zones Radiated by Thin Circular-Loop Antennas: A General Representation. *IEEE Trans. Antennas and Propagation*, 1997, vol. 45, no. 12, pp. 1741-1748.29.

27. Ahmet, S., Turk, A., Koksal Hocaoglu, Vertiy, A. Subsurface Sensing. *John Wiley & Sons, Inc.*, 2011, 960 p.

28. Melezhik, P. N., Morozov, V. Y., Poyedinchuk, A. Y., Mizrakhy, S. V., Nesterov, P. K, Vertiy, A. A. Numerical-analytical method for determining the

ISSN 1814-4225 (print)
ISSN 2663-2012 (online)

dielectric constant of 1d inhomogeneous plate in a waveguide. *IET Microwaves, Antennas & Propagation*, 2020, vol. 14, pp. 1878-1885.

29. Mook, G., Hesse, J., Uchanin, V. *Deep Penetrating Eddy Currents and Probes. Materials Testing*, 2007, vol. 49, no. 5, pp. 258-264.

30. Uchanin, V. Detection of the fatigue cracks initiated near the rivet holes by eddy current inspection techniques. *Transactions on Aerospace Research*, 2020, no. 1 (258), pp. 47-58.

Надійшла до редакції 4.02.2021, розглянута на редколегії 23.09.2021

ВИХРОСТРУМОВИЙ ТОМОГРАФ ДЛЯ ВІЗУАЛІЗАЦІЇ ТРІЩИН В АВІАЦІЙНИХ ЗАКЛЕПКОВИХ З'ЄДНАННЯХ

О. О. Вертій, В. М. Учанін, В. В. Павліков, С. С. Жила, О. О. Шматко, Е. О. Церне

Контроль форми підповерхневих шарів металевих виробів необхідний у багатьох технологічних процесах. Так, наприклад, в аерокосмічній техніці дуже важливо визначити наявність дефектів у двигунах літаків. Такі ж проблеми виникають у хімічній, енергетичній та інших галузях промисловості, які випускають високотехнологічне обладнання. Широко використовувані електромагнітні методи контролю дефектів металевих виробів зараз є методами, що дозволяють відновити невідому розподільну провідність у досліджуваній зоні металу за допомогою вимірювання електричних характеристик (рами, котушки), скануючи поверхневу зону металу, на якій реєструються електричні струми (вихрові струми). Детектор вихрового струму (зонд) - це пристрій, який індукує вихрові струми в металевих предметах, а потім виявляє магнітні поля, що створюються цими вихровими струмами. Магнітне поле створюється котушкою або набором котушок, через які проходить електричний струм, що змінюється в часі. Робочі частоти досить низькі, від кількох герц до кількох сотень кілогерц, тому об'єкти, що представляють інтерес, знаходяться в ближньому полі передавача. Враховуючи високу провідність досліджуваних зразків, можна визначити, що використовувані хвилі в металах розташовані в міліметровій смузі хвиль. Зображення за допомогою вихрового струму можна розглядати як зображення ближнього поля та пристрій, що дозволяє отримувати зображення за допомогою вихрового струму, як скануючий мікроскоп ближнього поля. Дана робота містить результати моделювання та експерименту, отримані під час мікроскопії металевих конструкцій з вихровим струмом у ближньому полі. Проведене моделювання показало, що описаний метод томографії дозволяє реконструювати зображення поперечних перерізів неоднорідностей розміщених під поверхнею металу. Частина ближнього розсіяного поля, що виходить на поверхню була використана в алгоритмі реконструкції в базовій формі. Оскільки просторовий період (відстань між лініями нульової фази) у складових просторового спектра знаходиться в міліметровій смузі хвиль (P = 1 мм для максимальних значень), відновлені зображення мають дуже високі просторові частоти, хоча довжина падаючого поля дуже велика.

Ключові слова: вихрострумова томографія; багаточастотний режим; підповерхневі зображення.

ВИХРЕТОКОВЫЙ ТОМОГРАФ ДЛЯ ВИЗУАЛИЗАЦИИ ТРЕЩИН В АВИАЦИОННЫХ ЗАКЛЕПОЧНЫХ СОЕДИНЕНИЯХ

А. А. Вертий, В. Н. Учанин, В. В. Павликов, С. С. Жила, А. А. Шматко, Э. А. Церне

Контроль формы подповерхностных слоев металлопродукции необходим во многих технологических процессах. Так, например, в авиакосмической технике очень важно определять наличие дефектов в двигателях самолетов. Такие же проблемы возникают в химической, энергетической и других отраслях промышленности, выпускающих высокотехнологичное оборудование. Широко применяемыми электромагнитными методами контроля дефектов в металлических изделиях в настоящее время являются методы, позволяющие восстановить неизвестную распределенную проводимость в исследуемой области металла по результатам измерения электрических характеристик (рамка, катушка), области сканирования на поверхность металла, в которой наводятся электрические токи (вихревые токи). Детектор вихревых токов (зонд) - это устройство, которое наводит вихревые токи на металлические предметы, а затем регистрирует магнитные поля, создаваемые этими вихревыми токами. Магнитное поле создается катушкой или набором катушек, через которые пропускается изменяющийся во времени электрический ток. Рабочие частоты достаточно низкие, от нескольких герц до нескольких сотен килогерц, поэтому интересующие цели находятся в ближнем поле передатчика. Учитывая высокую проводимость исследуемых образцов, можно определить, что используемые волны в металлах находятся в миллиметровом диапазоне. Вихретоковую визуализацию можно рассматривать как формирование изображения в ближнем поле, а устройство, позволяющее получать вихретоковые изображения, можно рассматривать как сканирующий микроскоп ближнего поля. Настоящая работа содержит моделирование и экспериментальные результаты, полученные при вихретоковой микроскопии металлических конструкций в ближней зоне. Проведенное моделирование показало, что описанный метод томо-

графии позволяет восстанавливать изображения поперечных сечений слабо рассеивающих неоднородностей, размещенных под поверхностью металла. В алгоритме реконструкции в основном использовалась часть ближнего обратно-рассеянного поля. Поскольку пространственный период (расстояние между линиями нулевой фазы) в компонентах пространственного спектра находится в диапазоне миллиметровых волн (P = 1 мм для максимальных значений), восстановленные изображения имеют очень высокие пространственные частоты, хотя длина падающего поля очень большая.

Ключевые слова: вихретоковая томография; многочастотный режим; подповерхностные изображения.

Вертій Олексій Олексійович – д-р физ наук, старш. наук. співроб., провідний науковий співробітник кафедри аерокосмічних радіоелектронних систем, Національний аерокосмічний університет ім. М. Є. Жуковського «Харківський авіаційний інститут», Харків, Україна.

Учанін Валентин Миколайович – д-р техн. наук, старш. наук. співроб., провідний науковий співробітник відділу №9 методів та засобів відбору й обробки діагностичних сигналів, Фізико-механічний інститут ім. Г. В. Карпенка НАН України, Львів, Україна.

Павліков Володимир Володимирович – д-р техн. наук, старш. наук. співроб., проректор з наукової роботи, Національний аерокосмічний університет ім. М. Є. Жуковського «Харківський авіаційний інститут», Харків, Україна.

Жила Семен Сергійович – д-р техн. наук, зав. каф. аерокосмічних радіоелектронних систем, Національний аерокосмічний університет ім. М. Є. Жуковського «Харківський авіаційний інститут», Харків, Україна.

Шматко Олександр Олександрович – канд. техн. наук, докторант каф. аерокосмічних радіоелектронних систем, Національний аерокосмічний університет ім. М. Є. Жуковського «Харківський авіаційний інститут», Харків, Україна.

Черне Едуард Олексійович – асист. каф. аерокосмічних радіоелектронних систем, Національний аерокосмічний університет ім. М. Є. Жуковського «Харківський авіаційний інститут», Харків, Україна.

Alexey Vertiy – D.Sc. in Radioengineering, National Aerospace University "Kharkiv Aviation Institute", Kharkiv, Ukraine,
e-mail: alexey.vertiy@gmail.com, ORCID: 0000-0002-9579-4709.

Valentyn Uchanin – D.Sc. in Radioengineering, Physico-Mechanical Institute of National Academy of Sciences of Ukraine, Lviv, Ukraine,
e-mail: vuchanin@gmail.com, ORCID: 0000-0001-9664-2101.

Vladimir Pavlikov – D.Sc. in Radioengineering, Vise rector for Science, National Aerospace University "Kharkiv Aviation Institute", Kharkiv, Ukraine,
e-mail: v.pavlikov@khai.edu, ORCID: 0000-0002-6370-1758.

Simeon Zhyla – D.Sc.in Radioengineering, Head of Department of Aerospace Radio-electronic Systems, National Aerospace University "Kharkiv Aviation Institute", Kharkiv, Ukraine,
e-mail: s.zhyla@khai.edu, ORCID: 0000-0003-2989-8988.

Olexandr Shmatko – PhD in Radioengineering, doctoral student of Department of Aerospace Radio-electronic Systems, National Aerospace University "Kharkiv Aviation Institute", Kharkiv, Ukraine,
e-mail: o.shmatko@khai.edu, ORCID: 0000-0002-3236-0735.

Eduard Tserne – Assistant of the department aerospace radio-electronic systems, National Aerospace University "Kharkiv Aviation Institute", Kharkiv, Ukraine,
e-mail: e.tserne@khai.edu, ORCID: 0000-0003-0709-2238.